Helmholtz-Zentrum
Geesthacht
Zentrum für Material- und Küstenforschung

Final Draft
of the original manuscript:

Goushegir, S.M.; dos Santos, J.F.; Amancio-Filho, S.T.:

Failure and fracture micro-mechanisms in metal-composite single lap joints produced by welding-based joining techniques

In: Composites / A (2015) Elsevier

DOI: 10.1016/j.compositesa.2015.11.001

Failure and fracture micro-mechanisms in metal-composite single lap joints produced by welding-based joining techniques

S.M. Goushegir[a], J.F. dos Santos[a], S.T. Amancio-Filho[a,b,*]

[a] Helmholtz-Zentrum Geesthacht, Centre for Materials and Coastal Research, Institute of Materials Research, Materials Mechanics, Solid State Joining Processes, Max-Planck-Str. 1, 21502, Geesthacht, Germany

[b] Hamburg University of Technology, Institute of Polymer Composites, Denicke Str. 15, 21073, Hamburg, Germany

[*] Corresponding author: Email: sergio.amancio@hzg.de Tel./Fax - +49 4152 87-2066 / -2033

Abstract

Welding-based joining technologies have been recently developed for metal-composite lightweight structures. In this work, the welding-based joining technology, friction spot joining, was selected to study the failure and fracture micro-mechanisms of an aluminum-composite single lap joint. Failure analysis suggested that the radial cracks nucleate at the periphery of the bonding area and propagate rapidly until failure of the so-called adhesion zone. Upon further loading the cracks propagate into the transition and plastically deformed zones leading to a reduction of the stiffness of the joint. The final stage of failure occurs rapidly in a catastrophic manner. The findings of the fractography using scanning electron microscopy demonstrated a mixed brittle-ductile fracture. Three zones were identified on the fracture surfaces: a smooth and featureless area known as the mirror zone demonstrating brittle fracture, a quasi-smooth area representing a mixture of ductile and brittle fractures and finally a zone with a highly rough surface implying ductile fracture of the composite part. Further, fiber pull-out and breakage were identified as additional fracture micro-mechanisms. All in all, metal-

composite joints produced by welding-based techniques demonstrate a mixed brittle-ductile fracture.

Keywords: A. Polymer-matrix composites (PMCs), B. Fracture, D. Fractography, E. Joints/joining

1. Introduction

Development of advanced materials with a diverse range of physical, chemical and mechanical properties such as lightweight metal alloys and fiber-reinforced polymer composites help designers to use the right combination of materials in the structures [1]. Various joining techniques are available for metal-polymer composite structures such as adhesive bonding [2, 3], different mechanical fastening processes [4-6], hybrid joining techniques [7-9] and recently welding-based joining methods. Among different technologies, welding-based metal-composite joining processes such as laser welding and direct joining [10, 11], induction welding [12], ultrasonic welding [13], and friction spot joining (FSpJ) [14] have been recently gaining more attention from transport industries. That is because of the advantages offered by these technologies over traditional adhesive bonding and mechanical fastening processes. Some of the main advantages include: very short joining cycles in the range of a few seconds, no essential need of using additional material (such as a fasteners) leading to weight saving, reduced stress concentration and susceptibility to cracking and delamination of the composite related to pre-drilling of a through-hole.

The feasibility and principles of the laser welding [10, 15] and laser direct joining [11, 16], induction welding [12] and ultrasonic welding [13, 17, 18], for different metal – thermoplastic composites were recently examined. The feasibility of the FSpJ was investigated for various combinations of metal – thermoplastic composites and the principles of the process described in terms of bonding mechanisms, microstructure and

mechanical performance of the joints [19-22]. Furthermore, the influence of process parameters on the mechanical performance and bonding area was addressed into details in [19, 23].

The influence of surface pre-treatments on the mechanical performance of the metal-composite joints [21, 24-26], their durability [27, 28] and fatigue performance [29] were also briefly reported in the literature. Despite the current knowledge on the physics of the processes and fundamental properties of welding-based metal-composite joints, there is still a lack of available information in the literature compared to the mature joining techniques such as adhesive bonding. This is in fact due to the earlier stage of development of the welding-based joining processes. The understanding of failure and fracture mechanisms is among the unexplored scientific subjects in welding-based joining technologies.

Single lap shear (SLS) geometry is widely used in the literature, due to its simplicity to evaluate mechanical performance and failure of the joints as well as to allow a direct comparison with state-of-the-art adhesive bonding and mechanical fastening. Although SLS geometry is simple to produce and test a joint it leads to a complex, mixed-mode loading scenario in the specimens [30]. Shear loading (Mode II) in combination with out-of-plane, normal forces (Mode I), as a result of the well-known secondary bending effect [30, 31], are the main loading types during SLS testing [30]. Due to the presence of load eccentricity in the SLS joint, a bending moment and a transverse load is generated as a result of the secondary bending to reduce the eccentricity [32, 33]. The bending of the joining parts and generation of transverse load leads to the formation of out-of-plane, normal stresses known as peeling stress [32]. Peeling stresses increase the stress concentration, especially at the ends (free edges) of the overlapped area, which reduces the mechanical performance of the joint. The influence of secondary bending

and the resultant peeling stresses have been widely studied for SLS adhesively bonded [30, 32, 34, 35] and mechanically fastened joints [31, 36]. In addition, Scanning electron microscopy (SEM) is frequently employed to investigate the fracture micro-mechanisms of bonded joints [37] as well as composite materials [38-41].

The initial attempts to investigate the fracture mechanisms of welding-based metal-composite joints showed a predominant mixed adhesive-cohesive fracture [12, 13, 19, 21, 22]. However there were no detailed analyses investigate failure and fracture micro-mechanisms. Therefore, in this work failure analysis and detailed SEM fractography of a metal-composite SLS joint produced by FSpJ process was performed. This welding-based technique was selected in this work for the production the SLS joints due to its increasing relevance for the academic and industrial communities [42-44]. Nevertheless, because of the shared similarities in bonding, failure and fracture mechanisms between FSpJ and other available welding-based joining processes, the findings of this work can be extended to other metal – thermoplastic composites joints.

2. Principles of the FSpJ process

The principles of the FSpJ process were thoroughly described in our previous publications [19, 21-23]. Briefly, the process is suitable for overlap configurations, whereby a metal sheet is placed on top of a polymer composite. A non-consumable tool consisting of three parts (a pin, a sleeve and a clamping ring (Figure 1a)) approaches the metal sheet while pin and sleeve rotate at the same direction. First, the rotating sleeve plunges to a pre-defined position without reaching the composite beneath the metal (Figure 1b-1) while pin retracts upward. As a result of the frictional heat generated between the metal and sleeve as well as axial forces exerted by the plunging motion of the sleeve, a volume of the metal around the tool is plasticized and flows in the cavity left behind by the retraction of the pin. Next, the pin pushes the plasticized metal to its

original position (Figure 1b-2). This leads to the deformation of the metal sheet at the interface with the composite in the form of an undercut known as a metallic “nub”. As a result of the axial forces the nub is slightly inserted into the composite leading to macro-mechanical interlocking between the joining parts. Simultaneously, the frictional heat is transferred from the metal to the composite via conduction. This leads to the local increase of the temperature, exceeding the melting temperature of the composite’s matrix, thereby a thin layer of the molten or softened polymer forms in the spot area. A part of this molten layer is squeezed out and flows laterally throughout the overlap region as a result of the axial pressure exerted by the tool. The molten layer is then consolidated under pressure, whereby it induces adhesion forces between the metal and composite. Finally, the tool retracts (Figure 1b-3) and the spot join consolidates.

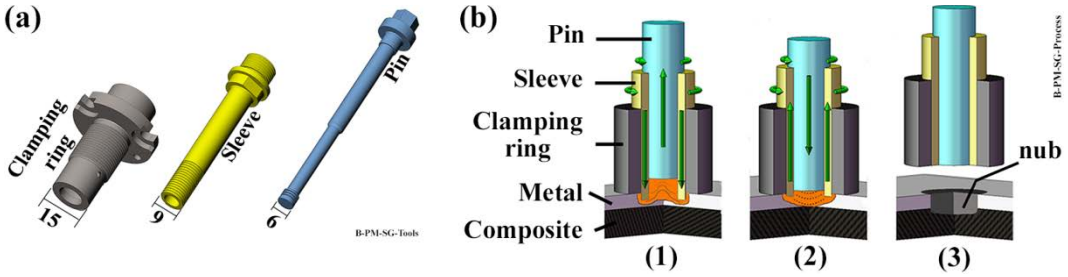

Figure 1 (a) FSpJ tool consisting of three parts (dimensions are in mm) and (b) process steps including: (1) the sleeve plunging softens the metal, (2) spot refilling, and (3) joint consolidation (adapted from[22]).

Figure 2a demonstrates a sound, consolidated metal-composite joint. A cross-section of the joint obtained from the middle of the spot is shown in Figure 2b, where the metallic nub is indicated.

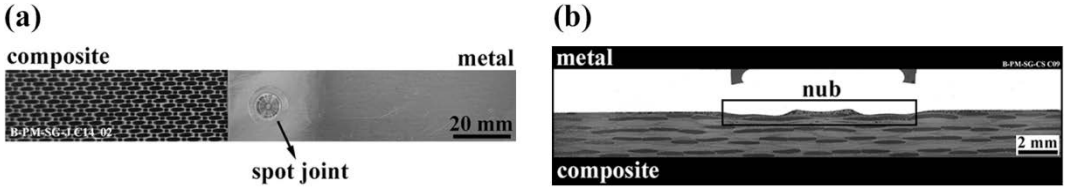

Figure 2 (a) Top view of a sound FSp join after consolidation and (b) a typical cross-section of a metal-composite FSp joint indicating the metallic nub.

In a previous work [21] we introduced a simple model to distinguish different bonding zones in an FSp joint. Figure 3 illustrates a typical fracture surface of an FSp joint divided into three bonding zones: an Adhesion Zone (AZ) related to the consolidated molten polymer, a Transition Zone (TZ) and a Plastically Deformed Zone (PDZ). PDZ was claimed to be the strongest part of the joint since different bonding mechanisms (i.e., mechanical interlocking and adhesion forces) act to hold the parts together. However, AZ and TZ are believed to be much weaker than PDZ due to the reduced adhesion forces and mechanical interlocking.

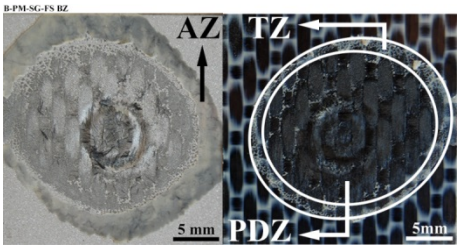

Figure 3 A typical fracture surface of an FSp joint illustrating different bonding zones.

3. Materials and methods

Aluminum alloy AA2024-T3 with a thickness of 2 mm (Constellium, France) was used as the metallic part. The nominal composition (wt%) of the alloy was 0.1 Si, 0.17 Fe, 4.55 Cu, 0.45 Mn, 1.49 Mg, <0.01 Cr, 0.16 Zn, 0.021 Ti and Al balance. Carbon-fiber-reinforced poly(phenylene sulfide) (CF-PPS) with a 2.17 mm nominal thickness consisting of 5 harness-woven quasi-isotropic laminates (TenCate, the Netherlands) with 50 vol% fibers was used as the composite partner. The composite consists of 7 plies of carbon fibers in the following sequence: [(0,90)/(±45)]3/(0,90). AA2024-T3 and CF-PPS were selected because of their applications in aircraft industry.

Both the aluminum and composite sheets were cut into 100 x 25.4 mm^2 coupon specimens for the joining process. The surface of the aluminum samples (in contact with the composite) was sandblasted prior to the joining process to increase surface roughness. The sandblasting was performed according to our previous work [21]. Moreover, both specimens were cleaned by acetone to remove surface contaminations prior to joining.

FSpJ was used to join the parts together. The process was optimized by means of design of experiments and analysis of variance for the selected joining materials and reported in [23]. The set of optimized joining parameters used in this work were: tool rotational speed of 2500 rpm, tool plunge depth of 0.8 mm, total joining time of 4 s and joining pressure of 3 bar.

SLS joints were produced with an overlap area of 25.4 x 25.4 mm^2. The produced FSp joints were then loaded, under lap shear tensile loading until failure, according to the ASTM D3163-01 [45] standard using universal testing machine (Zwick Roell model 1478) with a load capacity of 100 kN. The traverse test speed was 1.27 mm/min and the test was performed at room temperature. The obtained load-displacement curves were analyzed to understand the failure of the SLS joints. Additionally, both the aluminum and composite sides of the fractured joints were observed by SEM (Quanta^{TM} FEG 650 equipment) to investigate the fracture micro-mechanisms. For SEM analysis a voltage of 5 kV with a spot size of 3was used. The working distance was set approximately to 15 mm.

4. Results and discussion

4.1.Failure analysis

Figure 4 illustrates the fracture surface of a joint after SLS testing that is typical for FSpJ. It is clear from the figure that the FSp joints fail in shear mode through a mixed

adhesive-cohesive failure, which was also observed in other combinations of joining parts [19, 22] as well as other welding-based joining techniques [12, 13]. Further, it was explained [21] that in FSpJ radial cracks initiate at the periphery of the Adhesion Zone (AZ) and rapidly propagate until Transition Zone (TZ) under shear loading. Upon further loading the cracks start to propagate inside the first ply of the composite in the Plastically Deformed Zone (PDZ) [21]. Two primary cracking zones can be delineated during failure of an FSp joint as illustrated in Figure 4: crack initiation and propagation zones. The cracking zones can be correlated to the bonding zones as follows: crack initiation zone covers the AZ, whereas crack propagation zone can be divided into two regions. The first crack propagation zone takes place in the TZ and the second zone involves crack propagation in the PDZ. Such crack initiation and propagation behavior lead to a pure adhesive failure in the AZ, also known as interfacial failure [46]. However, cohesive failure was observed in the PDZ, in which a large amount of polymer matrix and carbon fibers remain attached to the aluminum surface (Figure 4). TZ shows a mixed adhesive-cohesive failure with the adhesive failure being more pronounced (Figure 4).

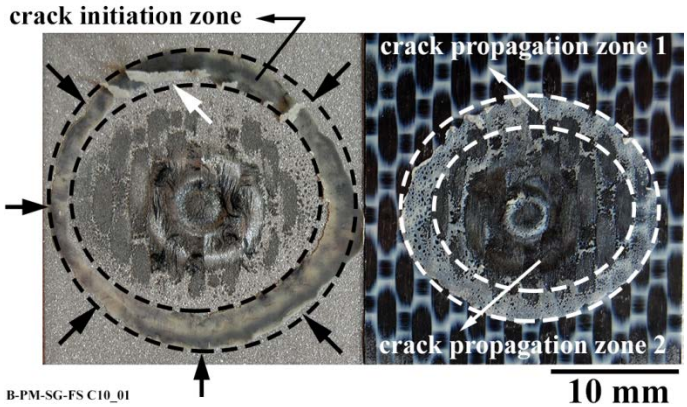

Figure 4 Fracture surface of an AA2024-T3 / CF-PPS FSp joint showing the initiation of radial cracks in the external periphery of the AZ. The white arrow indicates the influence of secondary bending on the tearing fracture of the PPS in the AZ.

It is also possible to observe in Figure 4 that a part of the AZ (indicated by a white arrow) has failed by tearing perpendicular to the loading plane. This might be an indication of the influence of secondary bending taking place close to the edge of the bonding area, which indeed reduces the lap shear strength of the joints.

To further evaluate the mechanical behavior of the joints, based on the failure mechanisms, one can analyze the load-displacement curve obtained from SLS testing of a joint. Figure 5 depicts a typical load-displacement curve for an FSp joint. It is obvious from the figure that FSp joints show a linear elastic behavior with limited failure displacement. The load-displacement curve can be divided into four zones. Zone 1 shows a linear elastic behavior with a high stiffness. This zone is relatively short and finishes when the radial cracks start to nucleate at the periphery of the AZ. Zone 2 corresponds to the propagation of the radial cracks until they reach the TZ, and the AZ has completely failed. This zone shows a reduced stiffness compared with Zone 1 as a result of crack propagation and loss of the AZ. Zone 3 illustrates a return to a quasi-linear elastic behavior with a slightly reduced stiffness compared to Zone 2 (see graph inset depicted in Figure 5). The beginning of the crack propagation in the TZ is the start of the third zone. The crack propagation in the TZ, PDZ and finally the area under the nub forms the third zone. The behavior of the joint in this zone is influenced by the secondary bending phenomenon. Similar behavior is reported by Olmedo *et al.* [31], where the stiffness of a bolted composite-composite single lap joint is highly influenced by the secondary bending phenomenon in different failure zones. The third zone ends

when the load reaches the ultimate lap shear strength of the joint. Finally, Zone 4 corresponds to the final catastrophic failure of the joint in a short fraction of a second.

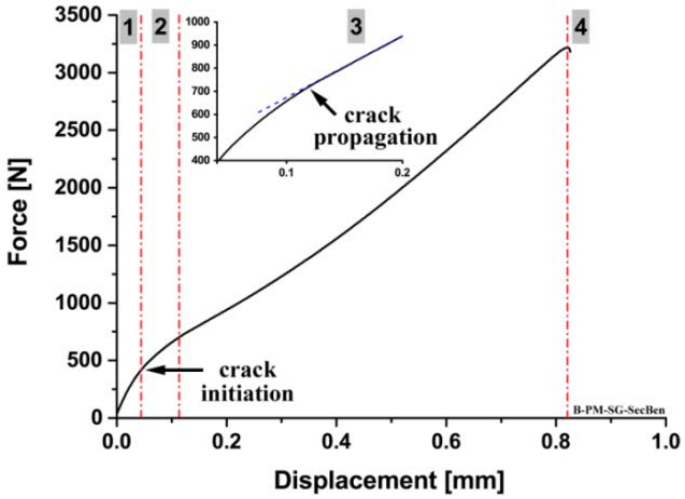

Figure 5 An example of the typical load (force) - displacement curve in FSpJ under shear loading divided into four regions. The graph inset shows a section of the curve related to the beginning of the crack propagation.

In order to further understand the characteristics of the FSp joint under lap shear loading, the behavior of the joint was simulated [47] by finite element analysis in Abaqus software. A snapshot of the simulation result is presented in Figure 6. This figure presents a cross-section of the joint to enable evaluation inside the overlap. As can be seen in the figure, the simulation result confirmed the occurrence of secondary bending at the ends of the joint, where both the aluminum and the composite are deflected to reduce load eccentricity. Deformation in the aluminum is expected to be higher due to its lower elastic modulus compared to CF-PPS, which leads to the formation of higher stress concentrations as can be seen in the simulation result. Large stresses form between the nub and the inner periphery of the AZ inside the overlap area. Premature failure of the joint may happen as a result of such stress concentration in a

region near to the metallic nub. Further simulation studies are in progress to better understand the behavior of SLS joints which will be published later.

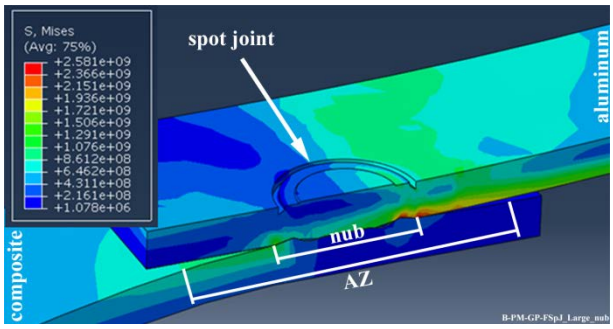

Figure 6 A cross-section snapshot of the AA2024-T3 / CF-PPS FSp joint simulated by finite elements analysis (traverse speed: 1.27 mm/min at room temperature). A region of high stress concentration inside the overlap area between the nub and the edge of the joint is visible. Adapted from [47].

4.2.Fractography

In this part, the involved fracture micro-mechanisms in each zone are discussed and related to three fracture zones based on roughness features explained by Kytopoulos *et al.* [48]: a very smooth area known as the mirror zone, a quasi-smooth (mist) zone, and a rough zone.

Figure 7 illustrates an overview of the AZ-TZ boundary both on the aluminum and composite surfaces. As can be observed from Figure 7a the AZ (on the aluminum surface) illustrates a very smooth, featureless area known as the mirror zone [48]. The AZ fails and detaches from the TZ by tearing, as shown by the arrows in the figure. Such a tearing failure is similar to those reported in [49] for ductile failure of thermoplastics. The tearing failure is characterized by a smooth area close to the failure site without any noticeable deformed structure (such as fibrils). The AZ on the composite side is depicted in Figure 7b where the crack initiation sites are indicated by

arrows. The cracks propagate between the consolidated molten PPS layer and the composite, thus no traces of the consolidated layer can be detected on the composite. Note that the color difference in Figure 7b between AZ and the CF-PPS surface is due to a manual contrast change, to enable the distinguishing of the AZ.

Stochastic crack propagation can be seen in the TZ where some of the PPS matrix remains attached to the aluminum in the form of individual islands (indicated by arrows in Figure 7c). The fracture analysis of the TZ on the composite side (Figure 7d) illustrates two primary features: elongated fibrous-like features as in [49] (indicated by the white arrow), and a vein-type feature (indicated by the black arrow), very similar to those reported by Tanniru *et al.* [50]. Figure 7e shows a higher magnification of the elongated fibrils (from the elongated fibrous-like region in Figure 7d) that indicates a ductile fracture. However, a high magnification of the vein-type features is given in Figure 7f and as is apparent in this figure, within the large vein-type features the surface is very smooth, which resembles a brittle fracture. Furthermore, on the edges of both features, tearing of the PPS is clearly visible. Very sharp and approximately flat edges, without any plastic deformation are the signs of a brittle tear fracture. Therefore, the TZ shows a quasi-smooth (mist) area [48] with a mixed brittle-ductile fracture.

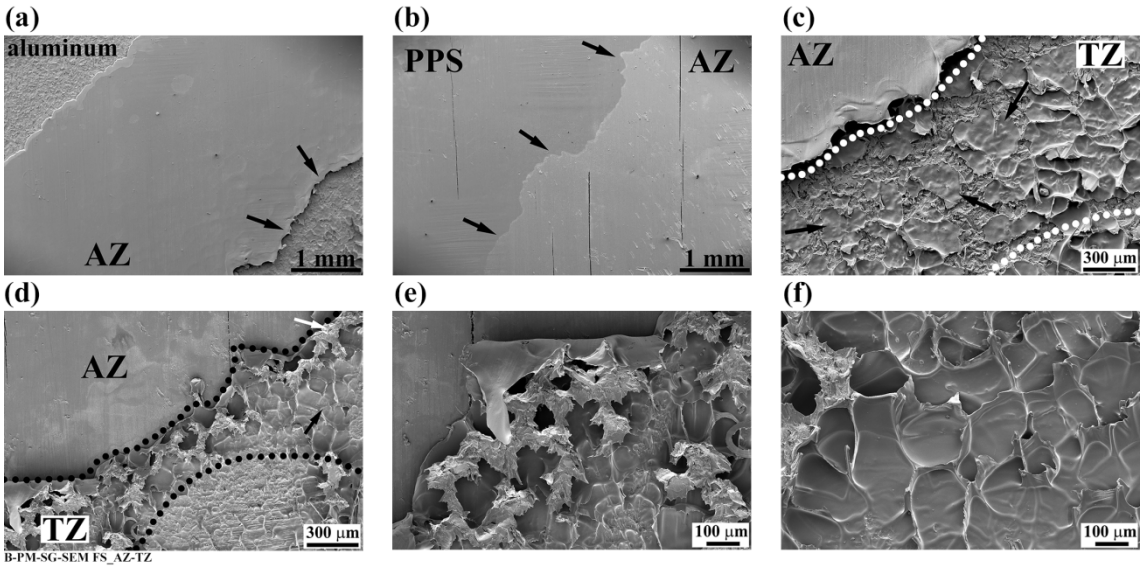

Figure 7 SEM fracture surface examination of the AA2024-T3 / CF-PPS FSp joint. (a) AZ on the aluminum, (b) AZ on the composite, (c) AZ-TZ boundary on the aluminum showing parts of the PPS remained attached as individual islands inside TZ, (d) AZ-TZ boundary on the composite showing fibrous-like (indicated by the white arrow) and vein-type (indicated by the black arrow) features in the TZ, (e) magnified image of the fibrous-like features implying a ductile fracture, and (f) magnified image of the vein-type features with a smooth area inside features implying a brittle fracture.

Turning now to the fracture mechanisms in the PDZ as the main crack propagation zone, Figure 8 displays the main features on the aluminum side. The SEM image of the nub area (as indicated by the circle in Figure 8a) is depicted in Figure 8b. It is visible from this figure that most of the surface of the aluminum is covered completely by the PPS. A fraction of the carbon fibers is also apparent, especially on the center of the spot. This is a clear indication that the cracks propagate inside the first ply of the CF-PPS. Fiber pull-out is another fracture micro-mechanism that was observed in the FSp joint. Figure 8c shows carbon fibers (indicated by the black arrows) that were pulled-out from the composite and remain attached to the aluminum surface. These fibers come from the warp direction in the composite, which were probably entrapped by the aluminum at the interface. Fiber-pull out is a well-known fracture mechanism in composites, which dissipates energy through fiber breakage and friction between the extracted fiber and matrix [51]. Fiber pull-out as a result of micro-mechanical interlocking was also reported by Balle *et al.* [13] in the ultrasonic welding of aluminum-carbon-fiber-reinforced plastic (CFRP). In addition to the pulled-out fibers, some of the PPS matrix was also detected on the aluminum. Figure 8d magnifies a part of the PPS matrix that remained on the aluminum as indicated by the rectangle in Figure 8c. Tearing of the PPS is one of the primary fracture micro-mechanisms apparent in the figure (indicated

by the black arrows). However, as indicated by the white arrow, a feature that resembles a drawing of the fibrils can also be seen, suggesting plastic deformation of the PPS. It seems that the PPS matrix is plastically deformed under complex combined shear and peeling stresses. As soon as the generated stresses exceed the local strength of the PPS, it fails through tearing. In addition to the warp fibers, fibers in the weft direction also contribute in the failure mechanisms. Figure 8e displays pieces of the weft fibers that are broken and remain attached to the aluminum. Since the weft fibers are perpendicular to the loading direction, when the local stresses exceed the transverse strength of the carbon fibers, fracture of the fibers occurs, leading to detachment of the fibers from the PPS matrix. Finally, as shown in Figure 8f areas with a very smooth, brittle fracture with micro-voids in the attached PPS material can be seen, especially inside the nub (Region 4). Since the micro-voids may act as stress concentration sites, micro-flaws originate from such voids. In areas where the density of the voids is high, coalescence of such micro-flaws leads to a very fast fracture in a brittle manner with a smooth appearance. The voids in this figure are believed to be formed during the FSpJ process as a result of air entrapment in the low viscosity PPS molten layer. We reported previously that the range of process temperature lies between 370°C and 474°C [23], being 437°C for the optimized joining condition used in this work. Because the achieved temperature is far below the onset of decomposition temperature for PPS (starting above 500°C as reported in [52, 53]), the observed defects (voids) are not related to the thermal decomposition. The absence of thermal decomposition during FSpJ was also confirmed through thermal analysis, however that results will be published in a separate document.

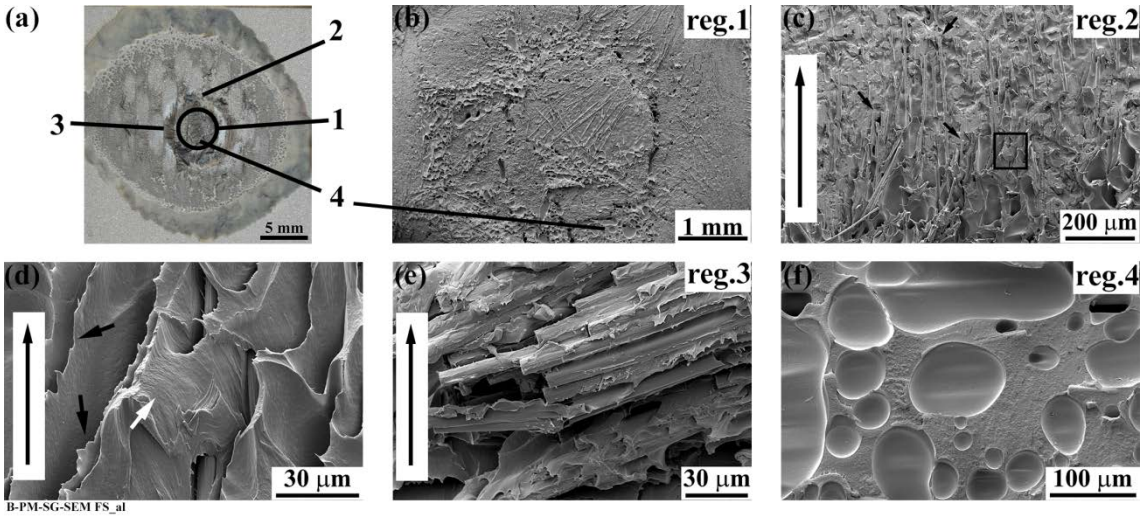

Figure 8 SEM fracture surface examination on the aluminum side from four regions indicated in (a), (b) general overview in the center of the spot showing PPS matrix and carbon fibers remained attached to the aluminum, (c) Pulled-out warp carbon fibers and parts of the PPS matrix attached on the aluminum, (d) high magnification image of the PPS matrix from (c) illustrating plastic deformation of the PPS (indicated by the white arrow) and tearing (indicated by black arrows), (e) Parts of the weft carbon fibers remained attached to the aluminum, while most of the fibers are partially covered by the PPS matrix, and (f) high magnification of a region with high concentration of voids showing very smooth, brittle fracture in the vicinity of the voids. Vertical arrows in (c), (d) and (e) show the direction of the applied load.

The main features of the composite fracture surface in the PDZ were examined in five regions as indicated in Figure 9a. Figure 9b reveals an overview of the spot area in which parts of the carbon fibers are shown to be slightly distorted, as indicated by arrows. Distortion of the fibers probably occurs during the joining process, due to the fact that the viscosity of the PPS is largely reduced and the molten PPS squeezed out of the region. As one of the roles of the matrix in composites is to tightly hold the fibers

together, an outward flow of molten PPS results in less matrix material around the carbon fibers, which can lead to slight distortion and rearrangement of the fibers.

The zone containing warp fibers (Figure 9c) shows a very rough surface involving large PPS fibrils elongated in the loading direction. The lengths of the fibrils were measured and they demonstrated a range between tens of microns to approximately 100 μm. In polymer composites a fibrous fracture with fibrils more than 10 μm in length implies ductile fracture [49]. Therefore, ductile fracture is the main feature mechanism in this area. In addition, tearing is shown to be the primary fracture micro-mechanism in this zone, which follows after the occurrence of a large plastic deformation of the PPS matrix. Tearing at the end of the fibril plastic deformation is shown in the high magnification image in Figure 9d. As discussed earlier, fiber pull-out is another fracture mechanism detected in the FSpJ as some of the warp fibers remain attached to the aluminum after the joint failure. The fiber pull-out mechanism can also be seen on the composite side as illustrated in Figure 9e. The white arrow in the figure shows a region (valley) were a fiber was pulled-out from the PPS matrix.

However, the area of the composite containing weft fibers shows mainly fractured fibers (Figure 9f). The weft fibers, which are aligned perpendicular to the loading direction, break when the local stress exceeds their transverse strength. A high magnification image of the broken weft fibers is depicted in Figure 9g. Some pieces of the fibers are bent in the direction of the applied load prior to their failure. The broken fibers remain attached to the aluminum as displayed in Figure 8e. Details of the fracture mechanism that takes place in the weft fibers are shown in Figure 9h. As indicated by the black arrows in this figure, micro-voids are generated at the fiber-matrix interface. Such micro-voids act as the origin of micro-cracks. The coalescence of such micro-cracks forms a larger crack that will propagate either along the fiber-matrix interface or into the

fiber. In cases of strong adhesion between carbon fibers and the PPS matrix, the transverse strength of the fibers is overcome as a result of high local stresses and so the crack propagates into the fiber, resulting in fiber fracture as shown in Figure 9g. However, if fiber-matrix adhesion is reduced (for instance by process-induced softening of the PPS matrix because of the high temperatures involved), the crack propagates at the fiber-matrix interface, leading to debonding and PPS matrix fracture by final tearing, as illustrated in Figure 9h. The crack propagation path is clearly apparent in the figure, as also indicated by the smaller white arrows (top of the figure). One can also see large plastic deformation of the PPS matrix and the tearing fracture along the fiber-matrix interface. The latter is indicated by larger white arrows (at the bottom) in the figure.

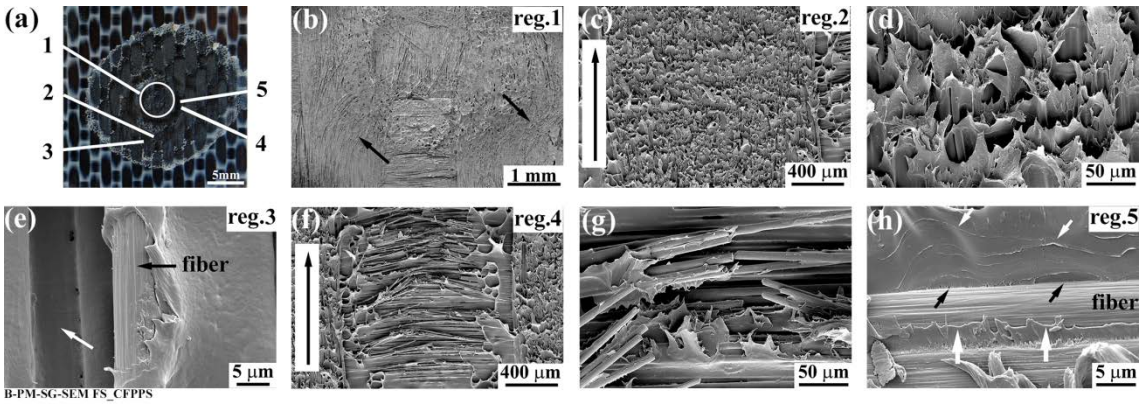

Figure 9 SEM fracture surface examination on the composite side from the regions indicated in (a), (b) general overview in the center of the spot where slight distortion of the fibers are indicated by the arrows, (c) elongated fibrils in an area containing warp fibers resembling a ductile fracture, (d) high magnification of the fibrils, where tearing fracture at the ends of the fibrils is apparent, (e) broken weft fibers, (f) high magnification of the broken weft fibers where slight rotation of the fibers in the direction of the applied load is visible. Direction of the applied load is indicated by the arrows in (c) and (f). (g) High magnification image of the warp fibers region in which the white arrow indicates an impression of a pulled-out fiber, and (h) high magnification

image of the fiber-matrix debonding in a weft fiber as a result of weakened fiber-matrix adhesion. Black arrows indicate some micro-voids acting as crack initiation, small white arrows show crack propagation path, and large white arrows illustrate tearing fracture along the fiber-matrix interface.

All in all, the SEM images reveal a three-dimensional rough surface in the PDZ on the composite side that resembles the rough area in the crack propagation zone as discussed by Kytopoulos *et al.* [48].

5. Conclusions

Failure analysis of the SLS metal-composite joint showed that radial cracks initiate at the outer periphery of the Adhesion Zone (AZ) followed by propagation into Transition Zone (TZ) and Plastically Deformed Zone (PDZ). The stiffness of the joint was reduced in two steps: firstly, when the radial cracks reach the TZ and the AZ is completely lost; secondly, when the cracks start to propagate into the TZ and PDZ. Most of the life of the joint corresponds to the crack propagation inside the PDZ. Generally, the SLS joint demonstrated a quasi-linear behavior with a final catastrophic failure with a limited elongation.

Detailed fractography by SEM revealed that the AZ is characterized by a very smooth, featureless area known as a mirror zone. The composite matrix did not show any deformation in the AZ, which resembles a brittle fracture. The TZ showed a mixture of an elongated fibrous-like region and a smooth veined-type area. Therefore, TZ is characterized by a quasi-smooth (mist) area and a mixture of ductile and brittle fractures. Finally, the PDZ showed a mixture of various fracture micro-mechanisms. Some of the warp fibers from CF-PPS were broken and pulled-out of the matrix. In addition, pieces of the weft fibers were broken and remained attached to the aluminum.

The composite matrix showed elongated fibrils in the direction of the applied load. The fibrils had a length of between tens of microns to approximately 100 microns, implying a ductile fracture. Fiber-matrix debonding was also detected in this zone. All in all, the failure micro-mechanisms in a metal-composite FSp joint demonstrated a mixture of ductile and brittle fracture, however the global failure behavior is governed more by the brittle fracture. Considering the similarities of the FSp joints with available welding-based joining process, the results of the present work may be extended to other welding-based technologies, contributing to the understanding of the failure and fracture mechanisms of metal-composite hybrid structures.

Acknowledgements

The authors would like to acknowledge the financial support of the Helmholtz Association through the Young Investigator Group, ‘‘Advanced Polymer Metal Hybrid Structures’’ (Grant No. VH-NG-626).

References

[1] Marsh G. Composites and Metals – A Marriage of Convenience? Reinforced Plastics. 2014;58:38-42.

[2] Matsuzaki R, Shibata M, Todoroki A. Reinforcing an aluminum/GFRP co-cured single lap joint using inter-adherend fiber. Composites: Part A. 2008;39:786-95.

[3] Rudawska A. Adhesive jointstrengthofhybridassemblies:Titaniumsheet-compositesand aluminium sheet-composites—Experimentalandnumericalverification. Int J Adhes Adhes. 2010;30:574-82.

[4] Abibe AB, Amancio-Filho ST, dos Santos JF, Hage Jr. E. Mechanical and failure behaviour of hybrid polymer–metal staked joints. Mater Des. 2013;46:338-47.

[5] Kabche JP, Caccese V, Berube KA, Bragg R. Experimental characterization of hybrid composite-to-metal bolted joints under flexural loading. Composites: Part B. 2007;38:66-78.

[6] Blaga L, Bancila R, dos Santos JF, Amancio-Filho ST. Friction Riveting of glass–fibre-reinforced polyetherimide composite and titanium grade 2 hybrid joints. Mater Des. 2013;50:825-9.

[7] Graham DP, Rezaei A, Baker D, Smith PA, Watts JF. The development and scalability of a high strength, damage tolerant, hybrid joining scheme for composite–metal structures. Composites: Part A. 2014;64:11-24.

[8] Matsuzaki R, Shibata M, Todoroki A. Improving performance of GFRP/aluminum single lap joints using bolted/co-cured hybrid method. Composites: Part A. 2008;39:154-63.

[9] Ucsnik S, Scheerer M, Zaremba S, Pahr DH. Experimental investigation of a novel hybrid metal–composite joining technology. Composites: Part A. 2010;41:369-74.

[10] Bergmann JP, Stambke M. Potential of laser-manufactured polymer-metal hybrid joints. Physics Procedia. 2012;39:84-91.

[11] Katayama S, Kawahito Y. Laser direct joining of metal and plastic. Scripta Materialia. 2008;59:1247-50.

[12] Mitschang P, Velthuis R, Emrich S, Kopnarski M. Induction Heated Joining of Aluminum and Carbon Fiber Reinforced Nylon 66. J Thermoplast Compos Mater. 2009;22:767-801.

[13] Balle F, Wagner G, Eifler D. Ultrasonic spot welding of aluminum sheet/carbon fiber reinforced polymer – joints. Mat-wiss u Werkstofftech. 2007;38(11):934-8.

[14] Amancio-Filho ST, dos Santos JF. Method for joining metal and plastic workpieces. European Patent No. EP2329905B1; 2012.

[15] Rodroguez-Vidal E, Lambarri J, Soriano C, Sanz C, Verhaeghe G. A combined experimental and numerical approach to the laser joining of hybrid Polymer – Metal parts. Physics Procedia. 2014;56:835-44.

[16] Jung KW, Kawahito Y, Takahashi M, Katayama S. Laser direct joining of carbon fiber reinforced plastic to zinc-coated steel. Mater Des. 2013;47:179-88.

[17] Balle F, Eifler D. Statistical test planning for ultrasonic welding of dissimilar materials using the example of aluminum-carbon fiber reinforced polymers (CFRP) joints. Mat-wiss u Werkstofftech. 2012;43(4):286-92.

[18] Balle F, Wagner G, Eifler D. Ultrasonic Metal Welding of Aliminium Sheets to Carbon Reinforced Thermoplastic Composites. Adv Eng Mat. 2009;11(1-2):35-9.

[19] Esteves JV, Goushegir SM, dos Santos JF, Canto LB, Hage Jr. E, Amancio-Filho ST. Friction spot joining of aluminum AA6181-T4 and carbon fiber-reinforced poly(phenylene sulfide): Effects of process parameters on the microstructure and mechanical strength. Materials and Design. 2014;66 (Part B):437-45.

[20] Andre NM, Goushegir SM, dos Santos JF, Canto LF, Amancio-Filho ST. On the Microstructure and Mechanical Performance of Friction Spot Joining with Additional Film Interlayer. Annual Conference of the Society of Plastics Engineers, ANTEC 2014. Las Vegas, CA2014. p. 1791-7.

[21] Goushegir SM, dos Santos JF, Amancio-Filho ST. Friction Spot Joining of aluminum AA2024/carbon-fiber reinforced poly(phenylene sulfide) composite single lap joints: Microstructure and mechanical performance. Mater Des. 2014;54:196-206.

[22] Amancio-Filho ST, Bueno C, dos Santos JF, Huber N, Hage Jr. E. On the feasibility of friction spot joining in magnesium/fiber-reinforced polymer composite hybrid structures. Mater Sci Eng A. 2011;528:3841-8.

[23] Goushegir SM, dos Santos JF, Amancio-Filho ST. Influence of process parameters on mechanical performance and bonding area of AA2024/carbon-fiber-reinforced poly(phenylene sulfide) friction spot single lap joints. Mater Des. 2015;83:431-42.

[24] Yusof F, Yukio M, Yoshiharu M, Abdul Shukor MH. Effect of anodizing on pulsed Nd:YAG laser joining of polyethylene terephthalate (PET) and aluminium alloy (A5052). Mats & Des. 2012;37:410-5.

[25] Esteves JV, Amancio-Filho ST, dos Santos JF, Canto LB, Hage Jr. E. Friction spot joining of aluminum 6181-T4 and carbon fiber reinforced poly(phenylene sulfide). 70th Annual Technical Conference of the Society of Plastics Engineers 2012, ANTEC 2012. Orlando, FL2012. p. 1698-704.

[26] Mitschang P, Velthuis R, Didi M. Induction Spot Welding of Metal/CFRPC Hybrid Joints. Adv Eng Mater. 2013;15(9):804-13.

[27] Roesner A, Olowinsky A, Gillner A. Long term stability of laser joined plastic metal parts. Physics Procedia. 2013;41:169-71.

[28] Didi M, Emrich S, Mitschang P, Kopnarski M. Characterization of Long-Term Durability of Induction Welded Aluminum/Carbon Fiber Reinforced Polymer-Joints. Advanced Engineering Materials. 2013;15:821-9.

[29] Balle F, Huxhold S, Wagner G, Eifler D. Damage Monitoring of Ultrasonically Welded Aluminum/CFRP-Joints by Electrical Resistance Measurements. Procedia Eng. 2011;10:433-8.

[30] Yeh HY, Tandjung D. Mixed Mode Fracture Analysis of the Lap Shear Specimen Test Per ASTM D1002. J Reinf Plast Comp. 2005;24:839-53.

[31] Olmedo A, Santiuste C, Barbero E. An analytical model for the secondary bending prediction in single-lap composite bolted-joints. Comp Struc. 2014;111:354-61.

[32] da Silva LFM, das Neves PJC, Adams RD, Spelt JK. Analytical models of adhesively bonded joints - Part I: Literature survey. Int J Adhes Adhes. 2009;29:319-30.

[33] Goland m, Reissner E. The Stresses in Cemented Joints. J Appl Mech. 1944;11:A17-A27.

[34] Lee HK, Pyo SH, Kim BR. On joint strengths, peel stresses and failure modes in adhesively bonded double-strap and supported single-lap GFRP joints. Comp Struc. 2009;87:44-54.

[35] da Silva LFM, P.J.C. das Neves PJC, Adams RD, Wang A, Spelt JK. Analytical models of adhesively bonded joints - Part II: Comparative study. Int J Adhes Adhes. 2009;29:331-41.

[36] Ekh J. Multi-Fastener Single-lap Joints in Composite Structures. Stockholm: PhD thesis, Royal Institute of Technology; 2006.

[37] Wilcox RC, Jemian WA. Scanning Electron Fractography of Lap-Shear Joints J Polym Eng Sci. 1973;13(1):40-5.

[38] Prabhakaran RTD, Pillai S, Charca S, Oshkovr SA, Knudsen H, Andersen TL, et al. Mechanical characterization and fractography of glass fiber/polyamide (PA6) composites. J Polym Comp. 2015;36(5):834-53.

[39] Schouwenaars R, Cerrud S, Ortiz A. Mechanical analysis of fracture in an automotive radiator head produced from a nylon-glass fibre composite. Composites: Part A. 2002;33:551-8.

[40] Silva H, Ferreira JAM, Capela C, Richardson MOW. Mixed Mode interlayer fracture of glass fiber/nano-enhanced epoxy composites. Composites: Part A. 2014;64:211-22.

[41] Yilmaz S, Yilmaz T. Effect of POSS and chain extender on tensile and fracture properties of neat and short glass fiber reinforced polyamide 6 composites. Composites: Part A. 2014;67:274-81.

[42] Amancio-Filho ST. Georg Sachs Prize. German Society for Materials Science (DGM); 2014.

[43] Amancio-Filho ST. AEE Rising Star / Innovation Star. Automotive Engineering Expo; 2015.

[44] Amancio-Filho ST, Goushegir SM, dos Santos JF. GHTC® - the German High Tech Champion Award 2013 in Lightweight Design. German Federal Ministry of Education and Research; 2013.

[45] ASTM D3163 - 01. Standard Test Method for Determining Strength of Adhesively Bonded Rigid Plastic Lap-Shear Joints in Shear by Tension Loading. ASTM International. 2008.

[46] Fessel G, Broughton JG, Fellows NA, Durodola JF, Hutchinson AR. Evaluation of different lap-shear joint geometries for automotive applications. Int J Adhes Adhes. 2007;27(7):574-83.

[47] Paz G, Blaga L, Goushegir SM, Abibe A, dos Santos JF, Mazzaferro J, et al. Numerical Simulation of the Mechanical Behavior of Polymer-Metal Joints. 21st CBECiMat, Brazilian Congress of Materials Science and Engineering. Cuiaba2014.

[48] Kytopoulos VN, Badalouka BG, Bourkas GD, Sideridis E. A SEM-Fractographic Study of Dynamic Crack Propagation Effects in Particulate Epoxy Systems under Impact Loading Conditions. J Reinf Plast Comp. 2009;28:353-77.

[49] Engel L, Klingele H, Ehrenstein G, Schaper H. Rasterelektronenmikroskopische Untersuchungen von Kunststoffschäden. München: Carl Hanser Verlag; 1978.

[50] Tanniru M, Yuan Q, Misra RDK. On significant retention of impact strength in clay-reinforced high-density polyethylene (HDPE) nanocomposites. Polymers. 2006;47:2133-46.

[51] Chawla KK. Composite Materials: Science and Engineering. Third ed. New York: Springer; 2012.

[52] Li XG, Huang MR, Bai H, Yang YL. High-Resolution Thermogravimetry of Polyphenylene Sulfide Film under Four Atmospheres. J App Poly Sci. 2002;83:2053-9.

[53] Ma CCM, Hsia HC, Liu WL, Hu JT. Thermal and Rheological Properties of Poly(Phenylene Sulfide) and Poly(Ether Etherketone) Resins and Composites. Poly Comp. 1987;8(4):256-64.